

# Energetic optimization of ion conduction rate by the K<sup>+</sup> selectivity filter

João H. Morais-Cabral\*, Yufeng Zhou & Roderick MacKinnon

Howard Hughes Medical Institute, Laboratory of Molecular Neurobiology and Biophysics, Rockefeller University, 1230 York Avenue, New York, New York 10021, USA

**The K<sup>+</sup> selectivity filter catalyses the dehydration, transfer and rehydration of a K<sup>+</sup> ion in about ten nanoseconds. This physical process is central to the production of electrical signals in biology. Here we show how nearly diffusion-limited rates are achieved, by analysing ion conduction and the corresponding crystallographic ion distribution in the selectivity filter of the KcsA K<sup>+</sup> channel. Measurements with K<sup>+</sup> and its slightly larger analogue, Rb<sup>+</sup>, lead us to conclude that the selectivity filter usually contains two K<sup>+</sup> ions separated by one water molecule. The two ions move in a concerted fashion between two configurations, K<sup>+</sup>-water-K<sup>+</sup>-water (1,3 configuration) and water-K<sup>+</sup>-water-K<sup>+</sup> (2,4 configuration), until a third ion enters, displacing the ion on the opposite side of the queue. For K<sup>+</sup>, the energy difference between the 1,3 and 2,4 configurations is close to zero, the condition of maximum conduction rate. The energetic balance between these configurations is a clear example of evolutionary optimization of protein function.**

The KcsA K<sup>+</sup> channel contains multiple K<sup>+</sup> ions in its conduction pore (Fig. 1a). One ion resides at the centre of a water-filled cavity located halfway across the membrane, and others are present in a narrow, 12 Å-long segment adjacent to the extracellular pore opening<sup>1</sup>. This narrow segment is the selectivity filter where K<sup>+</sup> ions, but not Na<sup>+</sup> ions, bind in a nearly dehydrated state.

The selectivity filter is the central structural element that defines a K<sup>+</sup> channel; its amino-acid sequence is conserved in all K<sup>+</sup> channels throughout nature (Fig. 1b). In the filter, four strands of sequence TVGYG, one contributed by each of the four subunits, are arranged with their carbonyl oxygen atoms pointed inward towards the ion conduction pathway. This arrangement creates four potential ion-binding sites into which a K<sup>+</sup> ion can bind in an essentially dehydrated state, surrounded by eight oxygen atoms from the protein. Here, we refer to these selectivity filter sites as positions 1–4, from outside to inside (Fig. 1b). The three outermost sites (positions 1–3) are formed exclusively by carbonyl oxygen atoms, whereas position 4, adjacent to the central cavity, is formed by four carbonyl oxygen atoms and four threonine side-chain oxygen atoms. In each of the four sites, a K<sup>+</sup> ion can potentially be held at the centre of a box, with one plane of four oxygen atoms above and one plane below the ion.

Potassium ions diffuse through the channel at rates approaching 10<sup>8</sup> ions s<sup>-1</sup> under physiological conditions. To catalyse such high diffusion rates, the selectivity filter must allow a K<sup>+</sup> ion to dehydrate, enter and cross the selectivity filter within about 10 ns. The aim of this study is to deduce the individual steps in translocation of the K<sup>+</sup> ion across the selectivity filter, to understand how this process can occur at such a high rate. We carried out electrophysiological and X-ray crystallographic measurements in parallel to determine ion-throughput rates and ion distributions in the selectivity filter over a wide range of ion concentrations. Our ability to reach a plausible mechanism for conduction through the filter comes from a comparative analysis of K<sup>+</sup> and Rb<sup>+</sup>. Rb<sup>+</sup> is known to permeate K<sup>+</sup> channels, but its conduction features are unusual<sup>2,3</sup>. We find that the unusual properties of Rb<sup>+</sup> conduction are mirrored by an anomalous distribution of Rb<sup>+</sup> compared with K<sup>+</sup> in the selectivity filter. This anomalous distribution provides the key to understanding the detailed mechanism of K<sup>+</sup> conduction.

## Rubidium ion

Single KcsA K<sup>+</sup> channels were reconstituted into planar lipid bilayers, and ionic currents were recorded in the presence of equal concentrations of RbCl on both sides of the membrane. Figure 2a shows the current measured at 180 mV as a function of Rb<sup>+</sup> concentration. The current increases steeply at low Rb<sup>+</sup> concentrations (steep regime), begins to level off between 30 and 50 mM, and then continues to increase in a nearly linear fashion (linear regime).

X-ray crystallography was used to estimate the distribution of Rb<sup>+</sup> ions in the selectivity filter and to investigate how the distribution changes as a function of Rb<sup>+</sup> concentration. Crystals of the KcsA K<sup>+</sup> channel (space group C2) were grown in solutions of varying Rb<sup>+</sup> concentration. At concentrations less than 150 mM, we replaced Rb<sup>+</sup> with Na<sup>+</sup> or *N*-methylglucamine (NMG) to maintain constant ionic strength. Data were collected on flash-frozen crystals at the synchrotron, and difference Fourier omit maps were calculated from data to 3.4 Å Bragg spacings (see Methods). One-dimensional maps of electron density sampled along the axis of the selectivity filter (electron density profiles) show clear maxima

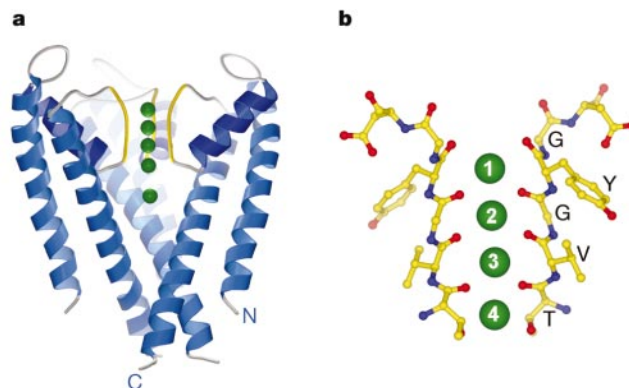


**Figure 1** Binding sites for K<sup>+</sup> ions in the KcsA K<sup>+</sup> channel. **a**, Ribbon representation of the KcsA channel with the subunit closest to the viewer removed. Potassium ions (green spheres) bind at four locations in the selectivity filter (yellow) and in the water-filled cavity at the membrane centre (bottom ion). **b**, Close-up view of the selectivity filter in ball-and-stick representation, with the front and back subunits removed. The four K<sup>+</sup> ions are numbered to indicate the location of binding sites in the filter; position 1 is closest to the extracellular solution and position 4 is closest to the cavity. Key amino acids forming the selectivity filter are shown. Pictures were prepared with GL-Render<sup>26,27</sup>.

\* Present address: Department of Molecular Biophysics and Biochemistry, Yale University, 260 Whitney Avenue, New Haven, Connecticut 06520, USA.

and minima (Fig. 2b). At the lowest concentration of Rb<sup>+</sup> (5 mM), there is a strong peak at each end of the selectivity filter, corresponding to positions 1 and 4, with a small peak near position 3. As the Rb<sup>+</sup> concentration is raised, the profile changes: the peak near position 1 nearly doubles in size, a large peak appears near position 3, while the peak near position 4 actually diminishes in size (Fig. 2b and c). No electron density peak appears at position 2 in the filter. Once a Rb<sup>+</sup> concentration of about 30 mM is reached, there is little further change in the electron density profile except for a gradual increase in the peak at position 4.

The first interesting aspect of the electron density profiles is that their dependence on ion concentration correlates well with the concentrations over which the steep and linear regimes of the conduction–concentration curve are observed. That is, the transition from the low-concentration profile (a peak at positions 1 and 4) to the high-concentration profile (large peaks at positions 1 and 3 with a smaller peak at position 4) matches the transition from steep to linear conduction regimes (Fig. 2a and c). The second interesting aspect is that the electron density transition from low (5 mM) to high ( $\geq 30$  mM) Rb<sup>+</sup> concentration clearly reflects an increase in the number of Rb<sup>+</sup> ions in the filter. This increase might at first seem to be a transition from two to three Rb<sup>+</sup> ions, but it is in fact more compatible with a transition from one to two ions. To see why this is so, imagine that when a single Rb<sup>+</sup> ion is in the filter it resides at either position 1 or 4, resulting in an occupancy of about 0.5 at each position, and that when two ions are in the filter they reside at positions 1 and 3, with an occupancy of 1.0 at each position. In this case, as the Rb<sup>+</sup> concentration is increased from low to high, and a growing fraction of channels go from having one ion to two ions in

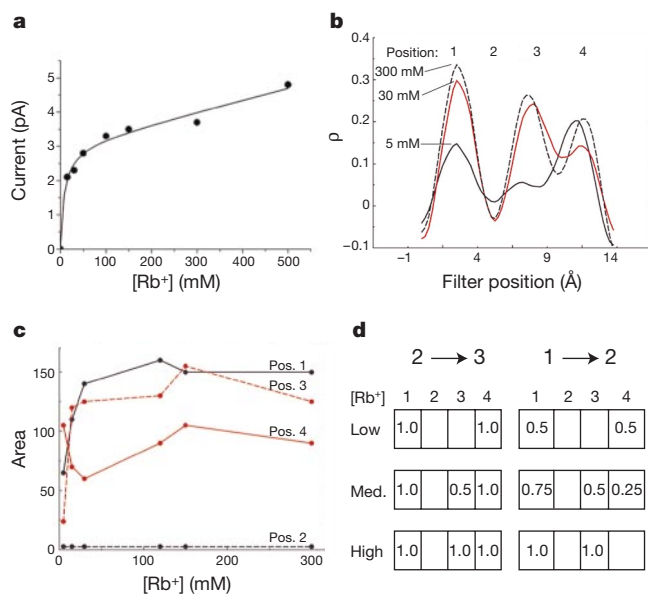


**Figure 2** Rubidium conduction and crystallographic distribution of Rb<sup>+</sup> ions in the selectivity filter. **a**, Currents recorded from single KcsA K<sup>+</sup> channels in the presence of equal concentrations of internal and external RbCl are shown as a function of ion concentration. Recording voltage was +180 mV. **b**, Electron density ( $\rho$ ) was sampled along the axis of the selectivity filter from difference Fourier omit maps (3.4 Å resolution, C2 crystal form) and is represented as one-dimensional profiles. Zero on the *x*-axis corresponds to the level of the  $\alpha$ -carbon of residue 79 (extracellular entryway to the filter). Profiles are shown for crystals grown in the presence of 5, 30 and 300 mM RbCl. Filter positions 1–4 are indicated. **c**, The area of peaks in the electron density profiles corresponding to selectivity filter positions 1, 2, 3 and 4 are shown as a function of the Rb<sup>+</sup> concentration in which the crystals were grown. **d**, Sets of boxes representing the four positions in the selectivity filter, with the Rb<sup>+</sup> ion occupancy shown for low, intermediate (med.) and high Rb<sup>+</sup> concentrations. Expected occupancies for transitions from one to two ions (right) and from two to three ions (left) are shown (see text).

the filter, occupancy at position 1 will increase from 0.5 to 1.0, occupancy at position 3 will increase from 0 to 1.0, and occupancy at position 4 will decrease from 0.5 to 0 (Fig. 2d, right). These changes in occupancy are in qualitative agreement with the concentration dependence of peaks in the electron density profiles (Fig. 2b and c). The increase at position 1 and decrease at position 4 observed in the electron density is important because it is not explained by the transition from two to three ions. Such a transition would require positions 1 and 4 to each have an occupancy of 1.0 at low Rb<sup>+</sup> concentrations; as Rb<sup>+</sup> concentration is raised, an increasing fraction of channels with three ions in the filter would be manifest as an increasing occupancy at position 3 and nothing more (Fig. 2d, left). This simple explanation captures the approximate features of the data. More detailed considerations (below) account for the fact that the peak at position 4 does not disappear altogether, and actually becomes a little larger as Rb<sup>+</sup> concentration is increased beyond 30 mM (Fig. 2b and c).

### Potassium ion

Potassium current through the KcsA K<sup>+</sup> channel is shown in Fig. 3a. As in the case of Rb<sup>+</sup>, K<sup>+</sup> conduction exhibits a steep regime at low ion concentrations and a linear regime at high concentrations. The striking difference between Rb<sup>+</sup> and K<sup>+</sup> is in the slope of the linear regime: the K<sup>+</sup> current continues to increase with ion concentration, whereas the Rb<sup>+</sup> current nearly levels off at a much smaller maximal value. This difference between Rb<sup>+</sup> and K<sup>+</sup> conduction has been documented previously and is a fairly general feature of K<sup>+</sup> channels<sup>2,3</sup>.

To study K<sup>+</sup> ions in the selectivity filter, we grew crystals in the presence of various K<sup>+</sup> concentrations. Two crystal forms (space groups C2 and I4) were analysed, and they yielded similar results (see Methods). Electron density profiles (I4 crystal form, 2.4 Å Bragg spacings) for the concentration range 3–200 mM K<sup>+</sup> are shown in Fig. 3b. The 3 mM K<sup>+</sup> profile is similar to the 5 mM Rb<sup>+</sup>

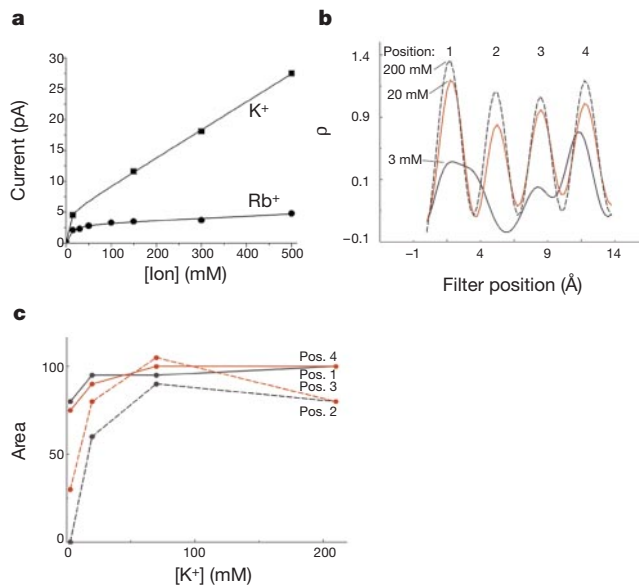


**Figure 3** Potassium conduction and crystallographic distribution of K<sup>+</sup> ions in the selectivity filter. **a**, Currents recorded from single KcsA K<sup>+</sup> channels in the presence of equal concentrations of internal and external KCl and RbCl are shown as a function of ion concentration. Recording voltage was +180 mV. **b**, Electron density ( $\rho$ ) was sampled as for Rb<sup>+</sup>-containing crystals, but the maps were calculated at 2.4 Å resolution from the I4 crystal form (see Methods). One-dimensional electron density profiles are shown for crystals grown in the presence of 3, 20 and 200 mM KCl. **c**, The area of peaks in the electron density profiles corresponding to selectivity filter positions 1, 2, 3 and 4 are shown as a function of the K<sup>+</sup> concentration in which the crystals were grown.

profile, showing a predominant peak on each end of the selectivity filter and a small peak near position 3 (Figs 2b and 3b). Therefore,  $\text{Rb}^+$  and  $\text{K}^+$  seem to be similar when only a single ion is present in the filter. However, as the  $\text{K}^+$  concentration is raised, a very significant difference between the  $\text{Rb}^+$  and  $\text{K}^+$  profiles emerges. Instead of the appearance of a large peak near position 3, as in  $\text{Rb}^+$ , two peaks appear at positions 2 and 3, yielding a profile with four roughly equal peaks. For both  $\text{Rb}^+$  and  $\text{K}^+$ , the transition from a low-concentration profile to a high-concentration profile occurs over a similar concentration range, 5–30 mM. Using the C2 crystal form, we found that the high-concentration profile in  $\text{K}^+$ , showing four approximately equal peaks, was unchanged in  $\text{K}^+$  concentrations of up to 500 mM (not shown).

Adjacent peaks in the  $\text{K}^+$  electron density profile are separated by about 3.2 Å (Fig. 3b). Potassium ions have a diameter of 2.7 Å, so they could, in principle, fit in the filter side by side, but this would seem to be an unstable binding configuration for electrostatic reasons. A survey of a database of small-molecule structure (Cambridge Crystallographic Data Centre, <http://www.ccdc.cam.ac.uk>) showed us that two  $\text{K}^+$  ions only very rarely occur with a separation distance of less than 3.5 Å. Therefore, although  $\text{K}^+$  ions may in principle occupy adjacent sites in the selectivity filter, we expect that most often they are separated by an intervening water molecule.

When comparing conduction data from channels in a bilayer with structural data from channels in a crystal, an important assumption is made: that ion distributions measured in the absence of a driving force (at equilibrium in the crystal) are relevant to currents measured in the presence of a driving force (with a voltage across the bilayer). The weak voltage dependence of  $\text{Rb}^+$  and  $\text{K}^+$  conductance (current per voltage) justifies this assumption. That is, the conductance measured at 180 mV is, within a reasonably small factor, equal to the conductance extrapolated to 0 mV, where the steady-state ion distribution in the pore must approach the equilibrium distribution. Consequently, the general features of the conduction–concentration curve for  $\text{K}^+$  channels, including KcsA, are similar near 0 and 200 mV for both  $\text{K}^+$  and  $\text{Rb}^+$  (ref. 3).

### Conduction mechanism

The key experimental observations in this study include the following. First, the electron density profile along the selectivity filter for both  $\text{Rb}^+$  and  $\text{K}^+$  ions undergoes a transition as the ion concentration is raised. The transition clearly demonstrates an increase in the number of ions in the selectivity filter, and, under physiological ion concentrations ( $>100$  mM  $\text{K}^+$ ), the filter operates by a multi-ion conduction mechanism. The transition is also correlated with a change in the conduction–concentration curve from a steeply rising regime at low ion concentrations to a shallower, roughly linear regime at high ion concentrations. Second, at low ion concentrations  $\text{Rb}^+$  and  $\text{K}^+$  have similar electron density profiles, but at higher concentrations they are different.  $\text{Rb}^+$  ions seem to prefer sites 1 and 3 in the filter, whereas  $\text{K}^+$  ions are more evenly distributed across all four sites. Third, at concentrations greater than about 50 mM, the occupancy and distribution of ions in the selectivity filter does not change much. The current, in contrast, continues to increase almost linearly, with a slope that is considerably steeper for  $\text{K}^+$  than for  $\text{Rb}^+$ .

It may seem that  $\text{Rb}^+$  and  $\text{K}^+$  ions permeate the  $\text{K}^+$  channel according to different rules, but a single model can account for the data, assuming a modest difference in the way  $\text{Rb}^+$  and  $\text{K}^+$  ions interact with the filter. Consider all possible states of the selectivity filter in which there can exist zero, one or two ions and in which ion pairs are separated by at least a single water molecule (Fig. 4a). The connecting lines, which indicate reversible kinetic pathways, imply concerted motions of ions and water. According to the X-ray data (Figs 2 and 3), even at low millimolar concentrations of  $\text{Rb}^+$  or  $\text{K}^+$ , there would have to be at least one ion in the filter residing close to

one of the ends (Fig. 4a, states G and H), perhaps with about half occupancy at each end. (In an accompanying paper, we show that the state of the selectivity filter at very low ion concentration is non-conductive<sup>4</sup>. For both  $\text{Rb}^+$  and  $\text{K}^+$ , conduction begins to occur as ion entry drives the channel out of this state.) As the ion concentration is raised, by mass action the filter will more probably be found in one of the three double-occupied states (Fig. 4a, states B, C and F). Next, suppose that when  $\text{K}^+$  is in the filter, the two double-occupied states B and C are equal in energy, and when  $\text{Rb}^+$  is in the filter, there is an energy difference between the states such that state C is less stable than state B. In this case the electron density for  $\text{K}^+$  would seem to be more or less evenly distributed over the filter, but for  $\text{Rb}^+$  the density at filter positions 1 and 3 would dominate. Furthermore, to the extent that state F occurs (the double-occupied state with an ion at positions 1 and 4), we might expect in high  $\text{K}^+$  to find the density at positions 1 and 4 to be a little stronger than at positions 2 and 3, and in high  $\text{Rb}^+$  to find a peak at position 4 in addition to the peaks at positions 1 and 3. The data show these features (Figs 2 and 3). We therefore suggest that  $\text{K}^+$  is very much like  $\text{Rb}^+$  in that two ions generally occupy the filter, but in the case of  $\text{K}^+$ , states B and C are energetically balanced, whereas in  $\text{Rb}^+$  they are not.

The above qualitative description is reinforced by quantitative analysis through a simulation of the state diagram (Fig. 4). The general features of ion occupancy (Fig. 4c and d) and conduction (Fig. 4b) for both  $\text{Rb}^+$  and  $\text{K}^+$  can be reproduced. More importantly, only a single parameter of the state diagram is changed to account for the difference between the two ions: for  $\text{Rb}^+$  there is a 5-kT energy difference between states B and C, whereas for  $\text{K}^+$  these states are equal in energy. Either relative destabilization of state C or

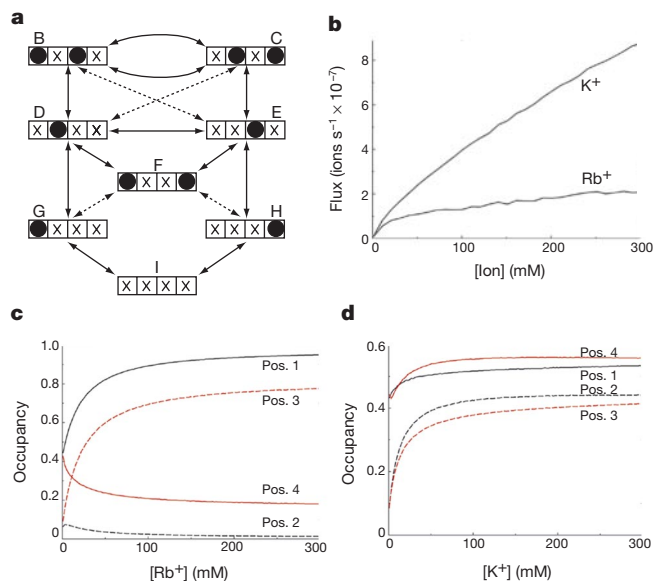


**Figure 4** Analysis of a conduction-state diagram constructed on the basis of the electron density profiles. **a**, Each set of four boxes (positions 1–4 from left to right) represents a state of the selectivity filter (left side outside the cell) with a specified configuration of ions (black circles) and water (crosses). The eight states, B–I, are the configurations of 0, 1 or 2 ions, assuming that ions are separated by at least a single water molecule. Arrows show the transition paths that connect the states through concerted movements of the ion–water queue (solid lines) or by ion–water exchange at the ends of the filter (dashed lines). Two paths connecting states B and C represent a concentration-independent movement of the ions from state B (1,3 configuration) to state C (2,4 configuration) and a concentration-dependent transition due to entry of a third ion on one side, causing exit of an ion on the opposite side. **b**, Simulated flux for  $\text{Rb}^+$  and  $\text{K}^+$ . **c**, **d**, Mean occupancies of selectivity filter position 1, 2, 3 and 4 are shown as functions of  $\text{Rb}^+$  (**c**) and  $\text{K}^+$  (**d**) concentration. Values of the rate constants for the state diagram are given in the Methods.

stabilization of state B generates a similar pattern of behaviour. The unexplained, gradual increase of the peak at position 4 in the data at high  $\text{Rb}^+$  concentrations (Fig. 2b and c) may reflect a measurable fraction of channels actually achieving a state of three  $\text{Rb}^+$  ions in the selectivity filter (see below).

The state diagram suggests a very plausible mechanism for the main  $\text{K}^+$  throughput cycle that occurs under physiological conditions (Fig. 4a). In the cellular environment, where the cytoplasmic  $\text{K}^+$  concentration is always high, the double-occupied states will predominate. A more detailed picture of the cycle connecting states B and C of Fig. 4a (hereafter referred to as the 1,3 and 2,4 configurations, respectively) is shown in Fig. 5a. The essential features of this cycle are that ions are separated by a single water molecule, that a queue of ions and water move in a concerted manner, and that exchange between the 1,3 and 2,4 configurations occurs either when the ion pair ‘jumps’ between configurations (concentration-independent path) or when a third ion enters on one side causing an ion to exit from the opposite side (concentration-dependent path). At an intuitive level, this mechanism makes good energetic sense. While in the 1,3 and 2,4 configurations, each  $\text{K}^+$  ion would reside near the centre of a box formed by eight oxygen atoms. Such coordination of single  $\text{K}^+$  ions by eight oxygen atoms is observed in the crystal structure of the  $\text{K}^+$ -selective antibiotic

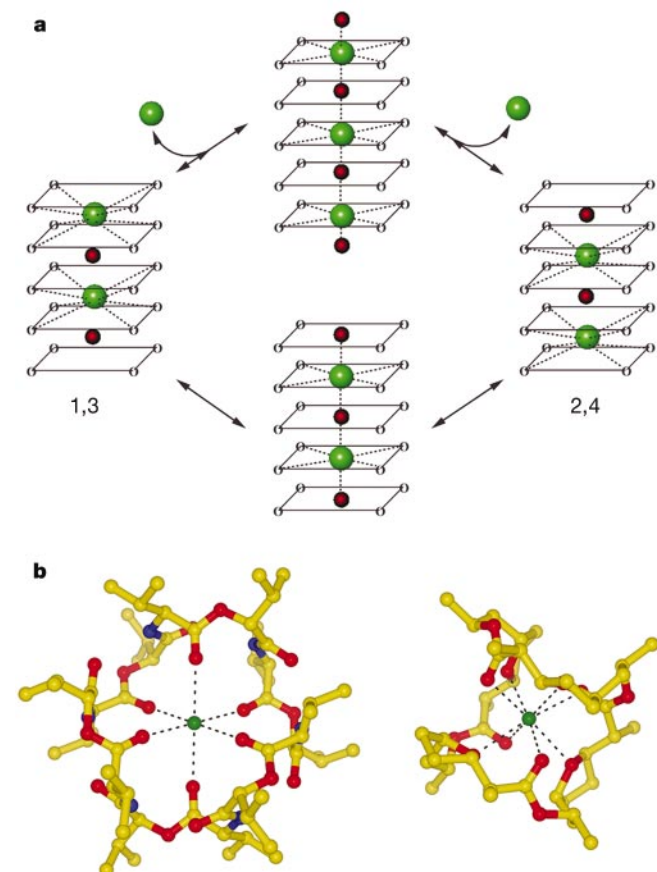


**Figure 5** The biologically important throughput cycle for  $\text{K}^+$  ions. **a**, Detailed description of the cycle connecting states B and C (Fig. 4a). The selectivity filter is depicted as five sets of four in-plane oxygen atoms (the top is outside the cell), with  $\text{K}^+$  ions and water molecules shown as green and red spheres, respectively.  $\text{K}^+$  ions undergo coordination by eight oxygen atoms when in the 1,3 and 2,4 configurations. Movement along either the concentration-independent path (bottom) or the concentration-dependent path (top) would involve octahedral coordination by six oxygen atoms, two provided by the intervening water molecules. **b**, The atomic structures of  $\text{K}^+$ -selective antibiotics nonactin (right) and valinomycin (left) exhibit coordination by eight and six oxygen atoms, respectively<sup>5–7</sup>.

nonactin (Fig. 5b, right)<sup>5,6</sup>. The inferred water molecule located between the ions provides a second analogy to another  $\text{K}^+$ -selective antibiotic, valinomycin (Fig. 5b, left)<sup>5,7</sup>. In valinomycin the  $\text{K}^+$  ion is coordinated in an octahedral manner, with four oxygen atoms in plane and one above and one below the ion. We imagine that during the transition between the 1,3 and 2,4 configurations a similar coordination is adopted transiently (Fig. 5a). These structural analogies to the  $\text{K}^+$ -selective antibiotics suggest that the transition between the 1,3 and 2,4 configurations occurs without a large energy barrier.

The 1,3 and 2,4 configurations leave one ‘free’ ring of oxygen atoms on the inside and outside end of the selectivity filter, respectively (Fig. 5a). The ‘free’ ring is therefore conveniently positioned to receive an incoming third  $\text{K}^+$  ion. Indeed, one may view the transition between the 1,3 and 2,4 configurations as the transfer of the ‘free’ oxygen ring from one end of the filter to the other, that is, a shuttling of the acceptor for the third  $\text{K}^+$  ion back and forth across the filter. The electron density profiles in  $\text{K}^+$  are consistent with an equal mixture of the 1,3 and 2,4 configurations and therefore the three-ion state is only implied by the cycle. (However, growth of the peak at position 4 in high  $\text{Rb}^+$  concentrations may reflect the three-ion state reaching a detectable occupancy in that case (Fig. 2b and c)). We hypothesize that the three-ion state would be somewhat higher in energy than the double-occupied states owing to electrostatic repulsion between ions and to the necessary dehydration and rehydration of entering and exiting ions, respectively. The three-ion state could be viewed as the transition state for the throughput cycle, in which case the filter ions may move back and forth between the 1,3 and 2,4 configurations many times along the concentration-independent path before the concentration-dependent path is taken. This picture predicts a linear regime of conduction because doubling the  $\text{K}^+$  concentration doubles the frequency of third ion entry (Figs 3a, 4b). At sufficiently high  $\text{K}^+$ , the concentration-independent path can, in principle, become rate limiting, at which point the current should approach a maximum value. The  $\text{Rb}^+$  data are interesting in this context. The energy difference between the 1,3 and 2,4 configurations inferred from the electron density profiles imposes a larger activation energy for going around the cycle (Fig. 6a). The lower current and shallower slope in the linear regime for  $\text{Rb}^+$  conduction therefore agrees well with the  $\text{Rb}^+$  electron density (Figs 2 and 4).

This conduction mechanism invokes the concerted movement of three  $\text{K}^+$  ions in the selectivity filter (two resident ions and one entering ion) in addition to the ion located in the cavity halfway across the membrane (Fig. 1). Measurements of unidirectional ion flux in  $\text{K}^+$  channels, and of ions interacting with blockers, have been used to estimate the number of ions seemingly present in the queue along the pore<sup>8–12</sup>. These independent approaches converge on a value of 3–4 ions, consistent with the conduction mechanism

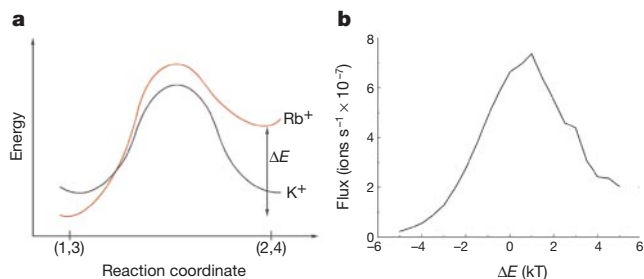


**Figure 6** Energetic optimization of  $\text{K}^+$  ion conduction. **a**, Hypothetical energy graph expresses the idea that the 1,3 and 2,4 ion configurations are energetically balanced ( $\Delta E = 0$ ) for  $\text{K}^+$  ions but imbalanced for  $\text{Rb}^+$  ions. **b**, Simulated flux for the state diagram (Fig. 4a) as a function of  $\Delta E$ , the energy difference between the 1,3 and 2,4 configurations. Flux corresponds to a 200 mM  $\text{K}^+$  concentration and 10-mV driving force. Rate constants are given in the Methods.

described here. Electrophysiologists have also addressed the question of how many water molecules move in an obligatory manner across the pore with a  $K^+$  ion. For technical reasons, this quantity is difficult to determine with great accuracy, but the number is estimated to be 1.0–1.5 water molecules per  $K^+$  ion<sup>13</sup>. Although the cavity at the membrane centre contains many water molecules in it, coupling of ions and water will be confined to the narrow selectivity filter. The throughput cycle described in Fig. 5a predicts one water molecule per  $K^+$  ion, in reasonable agreement with experiments.

### Energetic optimization of $K^+$ conduction rate

The crystallographic and electrophysiological differences between  $Rb^+$  and  $K^+$  in the channel have been attributed to the relative energies of the 1,3 and 2,4 configurations for these ions. The simulation shows that the main observable differences between  $Rb^+$  and  $K^+$  ions can be reproduced by simply imposing an energy difference between these configurations. We wondered whether it is a coincidence that the 1,3 and 2,4 configurations are balanced energetically in the case of  $K^+$ . There is no immediately apparent structural reason why this should be so. We propose that the observed balance is a consequence of evolutionary optimization of the rate at which ions diffuse through the pore. The basis for this proposal is simple: if the 1,3 and 2,4 configurations are imbalanced, the energy difference between them creates an inescapable energy step in the pathway around the throughput cycle. In terms of the diffusion rate, the energy step represents a kinetic barrier (Fig. 6a). Thus, by minimizing the energy difference between the 1,3 and 2,4 configurations through subtle adjustments of the protein structure, evolution has apparently minimized the kinetic barriers to achieve a high conduction rate (Fig. 6b). The channel did not evolve in response to the conduction of  $Rb^+$  ions, the slightly different radius of which apparently creates an imbalance with kinetic consequences.

### Summary

Our results lead us to conclude that, under physiological conditions, the  $K^+$  selectivity filter usually contains two resident  $K^+$  ions separated by a water molecule. The ion pair moves back and forth in a concerted manner between the 1,3 and 2,4 configurations until a third ion enters on one side, causing the displacement of an ion on the opposite side. The structure of the selectivity filter is designed by selection to have a maximum rate of conduction through minimization of the energy difference between the 1,3 and 2,4 ion configurations. □

### Methods

#### Crystal preparation

KcsA was prepared as described<sup>1</sup>. Protein was dialysed against a solution containing 5 mM lauryldodecylamine oxide (LDAO), 50 mM Tris buffer at pH 7.5, 2 mM dithiothreitol (DTT) and mixtures of NaCl, RbCl, KCl or NMG. For the growth of C2 crystals, 5 mM tetrabutylammonium chloride (TBA) was added to reduce crystal mosaicity and crystals were grown in sitting drops at 20 °C by equilibrating a 1 : 1 mixture of protein and reservoir solutions against the reservoir containing 50 mM HEPES buffer at pH 7.5, 120–300 mM  $CaCl_2$ , 35–50% PEG 400. Crystals were grown in the presence of 150, 300 or 500 mM KCl, 150 or 300 mM RbCl, 120 mM RbCl + 30 mM NaCl, 30 mM RbCl + 120 mM NaCl, 15 mM RbCl + 135 mM NMG and 5 mM RbCl + 145 mM NaCl. (Electron density maps from crystals containing NMG were consistent with those containing  $Na^+$  as the ion replacing  $K^+$ . This finding suggests that  $Na^+$  does not enter the selectivity filter.) Crystals of space group I4 were prepared as described<sup>4</sup>.

#### Crystallographic analysis

Data were collected on frozen crystals at X-25, National Synchrotron Light Source, Brookhaven National Laboratory; at A1 and F1, Cornell High Energy Synchrotron Source; at ID19, Advanced Photon Source, Argonne National Laboratory; and at ID13, European Synchrotron Radiation Facility (Table 1). Multiple data sets were collected from crystals at each ionic condition. The data were processed and reduced with Denzo and Scalepack<sup>14</sup>. For each ionic condition, the best data set was selected based on resolution,  $R_{\text{symm}}$  and signal-to-noise ratio. Further data processing was performed with the CCP4 program suite<sup>15</sup>. All C2 crystal form data sets were scaled against the 150 mM RbCl data set and sharpened (corrected for anisotropy)<sup>16</sup>.

Model refinement of the 150 mM RbCl and 150 mM KCl structures was carried out in

**Table 1** Diffraction data statistics

Salt condition	Resolution (Å)	$R_{\text{symm}}^*$ (%)	Completeness (%)
Space group C2			
RbCl 5 mM + 145 mM NaCl	3.45	10.7	86
RbCl 15 mM + 135 mM NMG	3.40	6.9	87
RbCl 30 mM + 120 mM NaCl	3.35	5.6	97
RbCl 120 mM + 30 mM NaCl	3.20	6.0	91
RbCl 150 mM	2.70	5.1	94
RbCl 300 mM	3.35	7.9	96
KCl 150 mM	2.80	7.2	93
Space group I4			
KCl 3 mM + 200 mM NaCl	2.30	5.6	99
KCl 20 mM + 180 mM NaCl	2.40	5.6	98
KCl 70 mM + 130 mM NaCl	2.20	5.4	100
KCl 200 mM	2.00	7.1	99

$$^*R_{\text{symm}} = \frac{\sum \Sigma(I) - I}{\Sigma(I)}$$

CNS with the published KcsA structure (Protein Data Bank accession code 1BL8) as an initial model<sup>17</sup>. After rigid body refinement, density modification by four-fold averaging and solvent flattening were applied before model rebuilding in program O<sup>15,18,19</sup>. Using data to 2.8 Å, we refined the  $Rb^+$  and  $K^+$  complex structures to an  $R_{\text{free}}$  of 30.2 and 32.2, respectively. These two models, together with the original KcsA structure, were then used for determination of electron density profiles along the selectivity filter. To remove model bias, the three models, without ions, were annealed at 2000 K against their corresponding data. Rigid body and positional refinement of the three models was then performed against the data set for each ion concentration. All three models were then put into the same coordinate file and used for the calculation of difference Fourier maps at 3.45 Å. We determined one-dimensional electron density profiles by sampling the difference maps along the central filter axis of the selectivity filter using MAPMAN<sup>20</sup>. To estimate the error contribution from Fourier series truncation (resolution limit), we analysed a model system of atoms in a queue with respect to the interatomic spacing and the resolution limit. We conclude that given the separation between ions in the filter, the 3.4 Å resolution limit introduces only relatively small errors in the magnitude of peaks and wells and allows us to define the ionic positions with accuracy.

All I4 crystal form data were scaled against the 200 mM KCl data set<sup>4</sup>. For the four  $K^+$  concentrations, models were refined without ions or water in the pore to an  $R_{\text{free}}$  in the range 24.2–26.2%; these models were used in the calculation of difference Fourier maps at 2.40 Å. To justify the comparison of electron density maps from the I4 and C2 crystal forms, especially as the C2 form contained a TBA cation in the cavity replacing the alkali metal cation normally present, several control data sets with  $K^+$  in the C2 form (50–500 mM), and one with  $Rb^+$  in the I4 form (200 mM) were studied. The electron density maps showed that the different crystal forms did not affect the distribution of ions in the selectivity filter, and that the comparison of maps is valid (not shown).

### Electrophysiological analysis

KcsA channels containing a six-histidine sequence on the carboxy terminus were purified and reconstituted into lipid vesicles as described<sup>21</sup>. Planar lipid bilayers of 1-palmitoyl-2-oleoyl phosphatidylethanolamine (POPE) (15 mg ml<sup>-1</sup>) and phosphatidyl glycerol (POPG) (Avanti Polar Lipids) (5 mg ml<sup>-1</sup>) in decane were painted over a 300-µm hole in a polystyrene partition separating internal and external solutions. To induce fusion of channel-containing vesicles, the external solution contained KCl or RbCl (150 mM) and HEPES (10 mM at pH 7.0) and the internal solution contained KCl or RbCl (20 mM) and succinate (10 mM at pH 4.0)<sup>22,23</sup>. Following channel fusion, the internal and external solutions were adjusted by solution addition or perfusion to achieve equal concentrations of KCl or RbCl. Membrane voltage was controlled and current recorded by an Axopatch 200B amplifier with a Digidata 1322A analogue-to-digital converter and Axoclamp software (Axon Instruments).

### Simulation of ion conduction

Ion conduction properties and ion probability distributions of the state diagram were analysed by a simulation in which a random variable with an exponential distribution was generated for each state<sup>24</sup>. Rate constants were expressed as an exponential function of energy<sup>25</sup>. Voltage dependence was applied to the rate constants by assuming that each ion crosses 0.2 of the membrane voltage difference when moving from one site to the next and when entering or exiting the filter, and that the energy barrier is located halfway between the sites. Values of the rate constants used in the simulation for  $K^+$  were (in units of  $M^{-1} s^{-1}$ ):  $k_{BA}, k_{CA}, 4 \times 10^9$ ;  $k_{DB}, k_{EC}, 1.6 \times 10^{10}$ ;  $k_{DB}, k_{EB}, 4 \times 10^{10}$ ;  $k_{CF}, k_{HE}, 2 \times 10^9$ ; (in units of  $s^{-1}$ )  $k_{AB}, k_{AC}, 1 \times 10^{11}$ ;  $k_{BC}, k_{CB}, 2 \times 10^9$ ;  $k_{BD}, k_{CE}, 5 \times 10^7$ ;  $k_{DE}, k_{ED}, 1 \times 10^9$ ;  $k_{DG}, k_{EH}, 1 \times 10^7$ ;  $k_{FE}, k_{FE}, 5 \times 10^9$ ;  $k_{FG}, k_{FH}, 1 \times 10^8$ ;  $k_{GD}, k_{HE}, 1 \times 10^6$ . The subscripts refer to the states in Fig. 4a, with state A representing the three-ion state connecting states B and C along the concentration-dependent path (Fig. 5a). The empty state was excluded from the simulation because it is not observed over the ion concentration range studied, and the pathways connecting states B to E and C to D were excluded for simplicity. For the  $Rb^+$  simulation, the network was modified by adjusting the value of a single parameter corresponding to the addition of 5 kT of energy to state C relative to its neighbouring states, maintaining detailed balance in the absence of a driving force. The simulation was carried out with a 10-mV driving force.

Received 2 August; accepted 10 September 2001.

- Doyle, D. A. *et al.* The structure of the potassium channel: molecular basis of K<sup>+</sup> conduction and selectivity. *Science* **280**, 69–77 (1998).
- Eisenman, G., Latorre, R. & Miller, C. Multi-ion conduction and selectivity in the high-conductance Ca<sup>2+</sup>-activated K<sup>+</sup> channel from skeletal muscle. *Biophys. J.* **50**, 1025–1034 (1986).
- LeMasurier, M., Heginbotham, L. & Miller, C. KcsA: It's a potassium channel. *J. Gen. Physiol.* **118**, 303–314 (2001).
- Zhou, Y., Morais-Cabral, J. H., Kaufman, A. & MacKinnon, R. Chemistry of ion coordination and hydration revealed by a K<sup>+</sup> channel–Fab complex at 2.0 Å resolution. *Nature* **414**, 43–48 (2001).
- Dunitz, J. D. & Dabler, M. in *Biological Aspects of Inorganic Chemistry* (eds Addison, A. W., Cullen, W. R., Dolphin, D. & James, B. R.) 113–140 (Wiley, New York, 1977).
- Dabler, v. M., Dunitz, J. D. & Kilbourn, B. T. Die struktur des KNCS-Komplexes von nonactin. *Helv. Chim. Acta* **52**, 2573–2583 (1969).
- Neupert-Laves, K. & Dabler, M. The crystal structure of a K<sup>+</sup> complex of valinomycin. *Helv. Chim. Acta* **58**, 432–442 (1975).
- Hodgkin, A. L. & Keynes, R. D. The potassium permeability of a giant nerve fibre. *J. Physiol. (Lond.)* **128**, 61–88 (1955).
- Begenisich, T. & De Weer, P. Potassium flux ratio in voltage-clamped squid giant axons. *J. Gen. Physiol.* **76**, 83–98 (1980).
- Bestergaard-Bogind, B., Stampe, P. & Christophersen, P. Single-file diffusion through the Ca<sup>2+</sup>-activated K<sup>+</sup> channel of human red cells. *J. Membr. Biol.* **88**, 67–75 (1985).
- Neyton, J. & Miller, C. Potassium blocks barium permeation through a calcium-activated potassium channel. *J. Gen. Physiol.* **92**, 549–567 (1988).
- Neyton, J. & Miller, C. Discrete Ba<sup>2+</sup> block as a probe of ion occupancy and pore structure in the high-conductance Ca<sup>2+</sup>-activated K<sup>+</sup> channel. *J. Gen. Physiol.* **92**, 569–586 (1988).
- Alcayaga, C., Cecchi, X., Alvarez, O. & Latorre, R. Streaming potential measurements in Ca<sup>2+</sup>-activated K<sup>+</sup> channels from skeletal and smooth muscle. *Biophys. J.* **55**, 367–371 (1989).
- Otwinowski, Z. & Minor, W. Processing of X-ray diffraction data collected in oscillation mode. *Methods Enzymol.* **276**, 307–326 (1997).
- Collaborative Computational Project, No. 4. The CCP4 Suite: Programs for X-ray crystallography. *Acta Crystallogr. D* **50**, 760–763 (1994).
- Gamblin, S. J., Rodgers, D. W. & Stehle, T. *Proc. CCP4 Study Weekend* 163–169 (Daresbury Laboratory, Daresbury, 1996).
- Brunger, A. T. *et al.* Crystallography & NMR system: A new software suite for macromolecular structure determination. *Acta Crystallogr. D* **54**, 905–921 (1998).
- Kleywegt, G. J. & Jones, T. A. in *From the First Map to Final Model. Proc. CCP4 Study Weekend* (eds Bailey, S., Hubbard, R. & Waller, D.) 59–66 (Daresbury Laboratory, Daresbury, 1994).
- Jones, T. A., Zou, J. Y., Cowan, S. W. & Kjeldgaard, M. Improved methods for building protein models in electron density maps and the location of errors in these models. *Acta Crystallogr. A* **47**, 110–119 (1991).
- Kleywegt, G. J. & Jones, T. A. xdlMAPMAN and xdlDATAMAN—Programs for reformatting, analysis and manipulation of biomacromolecular electron-density maps and reflection data sets. *Acta Crystallogr. D* **52**, 826–828 (1996).
- Heginbotham, L., LeMasurier, M., Kolmakova-Partensky, L. & Miller, C. Single streptomyces lividans K<sup>+</sup> channels. Functional asymmetries and sidedness of proton activation. *J. Gen. Physiol.* **114**, 551–560 (1999).
- Heginbotham, L., Kolmakova-Partensky, L. & Miller, C. Functional reconstitution of a prokaryotic K<sup>+</sup> channel. *J. Gen. Physiol.* **111**, 741–749 (1998).
- Cuello, L. G., Romero, J. G., Cortes, D. M. & Perozo, E. pH-dependent gating in the *Streptomyces lividans* K<sup>+</sup> channel. *Biochemistry* **37**, 3229–3236 (1988).
- Koonin, S. E. *Computational Physics* (Benjamin/Cummings, Menlo Park, 1986).
- Kramers, H. A. Brownian motion in a field of force and the diffusion model of chemical reactions. *Physica* **7**, 284–304 (1940).
- Kraulis, P. MOLSCRIPT: a program to produce both detailed and schematic plots of protein structures. *J. Appl. Crystallogr.* **24**, 946–950 (1991).
- Bacon, D. & Anderson, W. F. A fast algorithm for rendering space filling molecule pictures. *J. Mol. Graph* **6**, 219–220 (1988).

## Acknowledgements

We thank, for assistance, the staff at the National Synchrotron Light Source X-25; at Cornell High Energy Synchrotron Source, A1 and F1; at the Advanced Photon Source, ID19; and at the European Synchrotron Radiation Source, ID13. We thank Y. Jiang, R. Dutzler and A. Pico for assistance in data collection; B. Roux for discussions; and F. Valiyaveetil for discussion and advice on the manuscript. This work was supported by a grant from the National Institutes of Health to R.M. R.M. is an investigator in the Howard Hughes Medical Institute.

Correspondence and requests for materials should be addressed to R.M. (e-mail: mackinn@rockvax.rockefeller.edu). Coordinates have been deposited with the Protein Data Bank under accession codes 1JVM, 1K4C and 1K4D.